CORROSION SCIENCE AND TECHNOLOGY, Vol.20, No.5(2021), pp.249~255 pISSN 1598-6462 / eISSN 2288-6524
[Research Paper] DOI: https://doi.org/10.14773/cst.2021.20.5.249

Fabrication of a Porous Copper Current Collector Using a Facile Chemical Etching to Alleviate Degradation of a Silicon-Dominant Li-ion Battery Anode

Hongsuk Choi[1], Subin Kim[1], Hayong Song[1], Seokho Suh[2], Hyeong-Jin Kim[2,†], and KwangSup Eom[1,†]

[1]*School of Materials Science & Engineering, Gwangju Institute of Science and Technology (GIST), 123 Cheomdangwagi-ro, Buk-gu, Gwangju, 61005, Republic of Korea*
[2]*Graduate School of Energy Convergence, Gwangju Institute of Science and Technology (GIST), 123 Cheomdangwagi-ro Buk-gu, Gwangju 61005, Republic of Korea*
(Received July 28, 2021; Revised October 06, 2021; Accepted October 13, 2021)

In this work, we proposed a facile method to fabricate the three-dimensional porous copper current collector (3D Cu CC) for a Si-dominant anode in a Li-ion battery (LiB). The 3D Cu CC was prepared by combining chemical etching and thermal reduction from a planar copper foil. It had a porous layer employing micro-sized Cu balls with a large surface area. In particular, it had strengthened attachment of Si-dominant active material on the CC compared to a planar 2D copper foil. Moreover, the increased contact area between a Si-dominant active material and the 3D Cu could minimize contact loss of active materials from a CC. As a result of a battery test, Si-dominant active materials on 3D Cu showed higher cyclic performance and rate-capability than those on a conventional planar copper foil. Specifically, the Si electrode employing 3D Cu exhibited an areal capacity of 0.9 mAh cm^{-2} at the 300th cycles (@ 1.0 mA cm^{-2}), which was 5.6 times higher than that on the 2D copper foil (0.16 mAh cm^{-2}).

Keywords: *Lithium-ion battery, Copper current collector, Silicon-dominant anode, Porous structure, degradation*

1. Introduction

Lithium-ion battery (LiB) is a dominant energy storage system in the commercial field, especially for electric vehicles (EVs) and portable devices due to its high energy and power density [1-3]. As an anode material for LiBs, silicon (Si) is one of the most promising candidates because of its higher theoretical capacity (4200 mAh g^{-1}) and cost-effectiveness compared to graphite (372 mAh g^{-1}) dominantly used in the commercial field [4,5]. However, its large volume change (300~400 %) during the LiB cycling causes a severe degradation of a cell performance and a rapid decrease in the capacity through a pulverization of silicon particles and a delamination of active materials from the current collector (CC) [6,7]. To overcome this obstacle, many researchers have studied new synthesis and modification methods of a nanostructured silicon with high durability [8-11]. However, CC, which significantly affects the performance of silicon electrode as an important component of electrode, has been rarely studied. However, some studies reported that the modification of CC improved the durability and performance of Si-based electrode [12,13]. For example, silicon/graphite composite anode employing the nodule-type CC showed a higher cycle stability than that on a flat CC [12]. Moreover, thin silicon film sputtered on the porous Cu substrate showed a better electrochemical performance than that on the flat Cu substrate, because the porous structure relieved the stress on the silicon anode during cycling [13]. Unfortunately, however, since the modification methods reported in the above studies were based on compact film such as nodule-type Cu film or thin film process such as magneton sputtering, they are inappropriate in a high loading of active materials, although it is very critical to use the electrode practically. Therefore, alternative method to modify the surface of CC, which can facilitate a high-loading of active material of Si, and moreover can be fabricated by a facile method, is necessary. Herein, we introduce a facile two-step surface treatment using chemical oxidation and thermal reduction to make the 3D-structured Cu CC (3D Cu), and investigate the effects on the electrochemical performances and stability in terms of surface analysis, material characterization, and electrochemical impedance analysis.

[†]Corresponding author: hjkimc@gist.ac.kr and keom@gist.ac.kr
Hongsuk Choi: MS, Subin Kim : Ph.D. Student, KwangSup Eom and Hyeong-Jin Kim: Professor, (H. Choi and Subin Kim are co-first authors)

2. Experimental Methods

2.1 Synthesis of 3D Cu

First, NaOH (*Daejung Chemicals & Metals*) and ammonium persulfate (APS, *Duksan Pure Chemicals*) were dissolved in distilled water to prepare 10.0 M NaOH and 1 M APS solution, respectively. Second step was mixing 24 mL of NaOH, 12 mL of APS and 54 mL of distilled water. After making the solution, a copper foil was cleaned with 1 M HCl solution several times. After drying the foil, the enamel polisher was coated one side of the foil. The foil was immersed in the as-prepared solution for 12 hours. After that, the foil was cleaned by distilled water, acetone and ethanol. After drying the foil for an hour in room temperature, it was heated at 400 ºC for 10 hours in a H_2/Ar (5 v% of H_2) to make 3D Cu.

2.2 Materials characterization

X-ray diffraction (XRD) was conducted to characterize the crystal structure of the materials using a *D/MAX 2500V X-ray diffractometer system* (*Rigaku*) with Cu Kα radiation in the range of 25º-85º. Scanning electron microscopy (SEM) images for the copper foils were taken using a *Hitachi S-4700 Field Emission Scanning Electron Microscope (FESEM)* and a *JEOL IB-09020CP cross section polisher (CP).*

2.3 Electrochemical measurements

The slurries for the Si anodes were made of 70 wt% Si powder (*CNvision*), 20 wt% polyacrylic acid (*Sigma Aldrich*) and 10 wt% SuperC65 (*MTI*) as conductive additive. The obtained slurries were coated onto planar copper foil (2D Cu) and 3D Cu, respectively. These electrodes were dried overnight at 60 ºC. The electrochemical performances of Si half-cells were examined using 2032 coin-type cells. Each cell consisted of Si on 2D Cu and 3D Cu as the working electrode, a Li disk as the counter electrode, 1 M $LiPF_6$ solution in an EC/DEC solvent (1:1 by volume) with 10 wt% fluoroethylene carbonate as the electrolyte, and a Celgard 2400 as the separator. The coin cells were fabricated in the glove box with Ar atmosphere. Galvanostatic charge/discharge test, rate capability test, cyclic voltammetry (CV) tests were conducted using a battery charge/discharge cycler *(WonATech)*. The voltage window in every electrochemical test was 0.05-2.0 V (vs. Li^+/Li). Electrochemical impedance spectroscopy (EIS) was conducted over a frequency range from 1 mHz-100 kHz and a voltage amplitude of 10 mV via *VSP* potentiostat *(Bio-Logics)*. The areal loading masses of Si active materials were 1.0 ± 0.1 mg cm^{-2}. In the electrochemical tests, specific capacity and areal capacity were calculated based on the mass of Si.

3. Results and Discussion

Fig. 1 shows process of 3D Cu fabrication by a facile two-step synthesis including chemical oxidation and thermal reduction. In the chemical oxidation step, the shape of the oxidized copper at the surface of foil are dependent upon the concentration of the reactants, so the ratio of the reactants and etching time were selected to obtain flower-like morphology [14-16]. At the next step, thermal reduction, the CuO layer

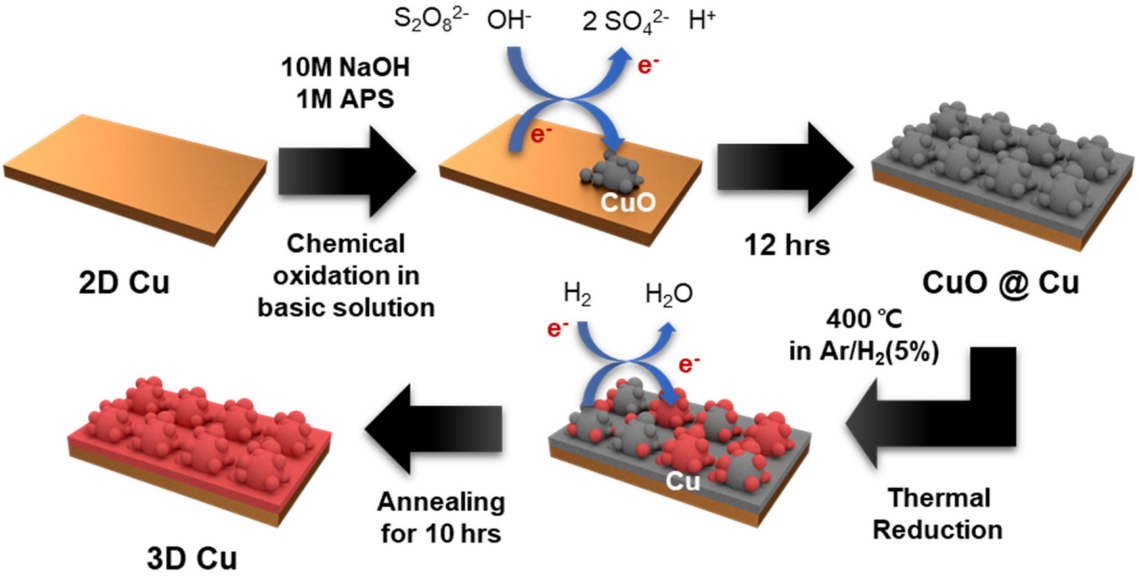

Fig. 1. The fabrication method of 3D Cu current collector using chemical oxidation and thermal reduction, proposed in this work

reacts with H_2 and successfully reduced to porous 3D Cu [17,18]. The accompanying chemical reactions during chemical oxidation and thermal reduction are described by Eqution (1) and Eqution (2). In alkaline solution, surface oxidation of copper into CuO could occur by Eqution (1). During thermal reduction, surface CuO layer reacts with H_2, producing water vapor and 3D Cu corresponding to Eqution (2).

$$\text{CuO layer formation: } Cu + 4\ NaOH + (NH_4)_2S_2O_8 \rightarrow CuO + 2\ Na_2SO_4 + 2\ NH_3 + 3\ H_2O \quad (1)$$

$$\text{Thermal reduction of CuO: } CuO + H_2 \rightarrow Cu + H_2O \quad (2)$$

In Fig. 2, the diffraction pattern shows that the surface of Cu is successfully oxidized to CuO, and CuO is converted to 3D Cu during subsequent thermal reduction. It is confirmed by removal of several CuO peaks after thermal reduction. To investigate the morphological change of Cu current collector during fabrication process, the surface SEM images are taken and shown in Fig. 3. 2D Cu (a) has flat surface than other samples. The surface of CuO @ Cu (b) is covered by the CuO flower balls consisted of several CuO sheets. The size of a CuO flower ball is 3-5 μm. Thermal reduction converts the CuO flower balls into the porous Cu balls successfully, and 3D Cu (c-d) is successfully fabricated. The size of a porous Cu ball is 3-5 μm, which is similar with a CuO flower ball. From the cross-sectional SEM of (e) 2D Cu and (f) 3D Cu, we could confirm that 3D Cu has much higher surface area than 2D Cu, so it could contribute to more contact points between active materials and CC. The size of a porous Cu ball is 3-5 μm and the thickness of the porous layer is about 10.6 μm.

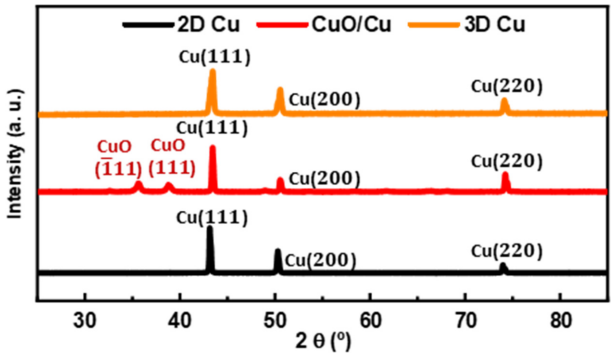

Fig. 2. XRD diffraction pattern of 2D Cu, CuO/Cu and 3D Cu

Fig. 4a-b show the CV plots of Si on 2D Cu and 3D Cu, which is similar to the plots in the previous paper. The scan rate at the first two cycles is 0.10 mV s^{-1} and the scan rate at the 3rd, 4th, 5th and 6th cycles are 0.15, 0.20, 0.25 and 0.30 mV s^{-1}, respectively. The number of an anodic peak and the number for a cathodic peak are same as one. These peaks are related with lithiation/delithiation of silicon anodes [19]. Both anodic peaks of 2D Cu and 3D Cu are based on the Li alloying peaks at 0.05-0.30 V. The cathodic peaks of 2D Cu are shown at 0.556 V and 0.599 V at the scan rate of 0.10 mV s^{-1} and 0.30 mV s^{-1}, respectively. The cathodic peaks of 3D Cu are shown at 0.520 and 0.576 V at the scan rate of 0.10 mV s^{-1} and 0.30 mV s^{-1}. The voltage of cathodic peaks of 2D Cu are higher than 3D Cu at every scan rates because of the higher overpotential at 2D Cu. The specific currents of every peaks at every cycles at 3D Cu are higher than that at 2D Cu. From the results of CV, we could expect that 3D Cu increases the electrical conductivity of electrode, which leads to the high specific capacity at the high current

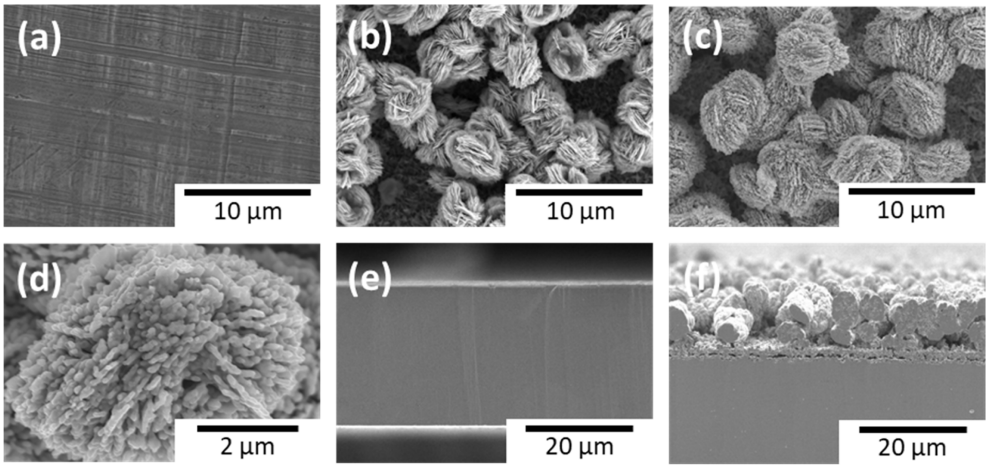

Fig. 3. SEM surface images of 2D Cu, CuO@Cu, and 3D Cu; (a) 2D Cu, (b) CuO @ Cu, (c-d) 3D Cu. Cross-sectional SEM of (e) 2D Cu and (f) 3D Cu

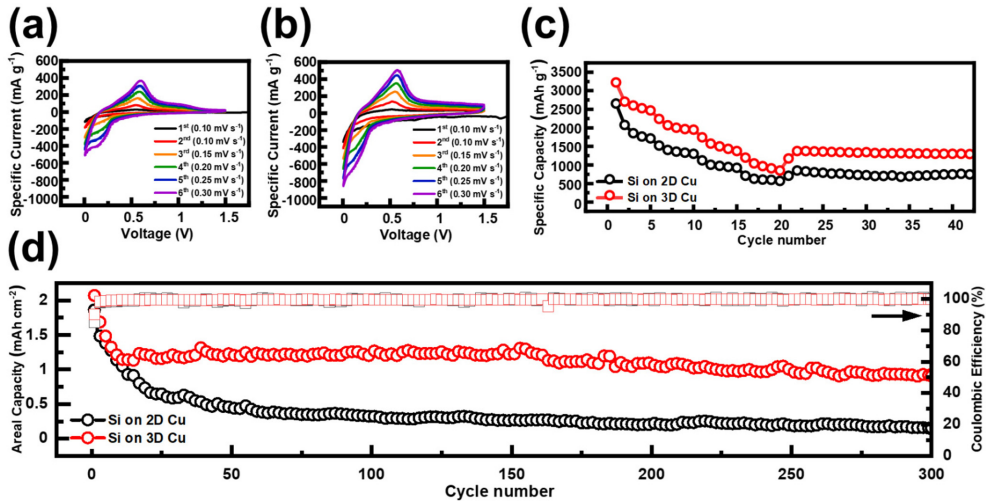

Fig. 4. Electrochemical performances of Si on 2D Cu and 3D Cu; (a) CV plots of 2D Cu and (b) 3D Cu, (c) rate capabilities of 2D Cu and 3D Cu at various current densities (0.25 A g^{-1}, 0.50 A g^{-1}, 1.0 A g^{-1}, 2.0 A g^{-1} for 5 cycles, 1.0 A g^{-1} for the other cycles), (d) cycle stabilities of 2D Cu and 3D Cu without the first 5 cycles (0.25 mA cm^{-2} for 5 cycles, 1.0 mA cm^{-2} for the subsequent cycles)

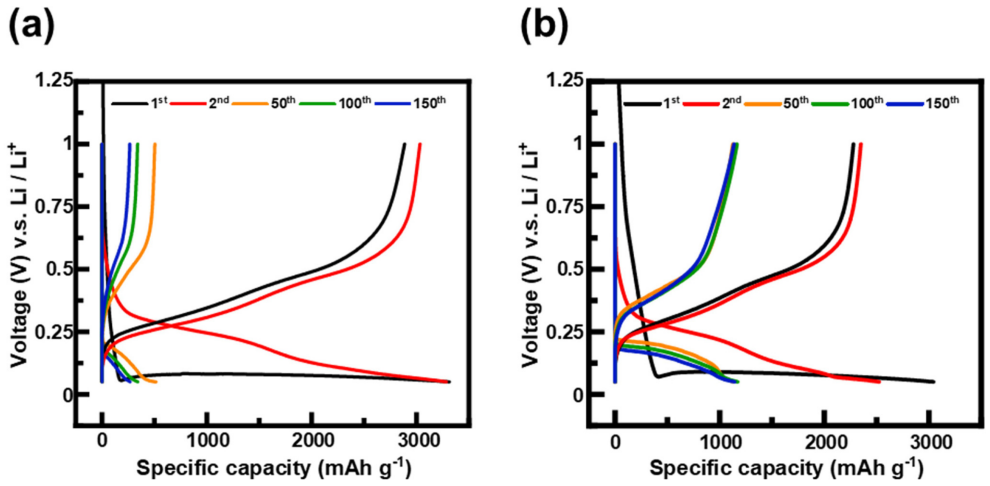

Fig. 5. Charge/discharge profiles of the Si anodes on 2D Cu and 3D Cu; (a) 2D Cu, (b) 3D Cu. (Current densities at 0.25 mA cm^{-2} for first 5 cycles, 1.0 mA cm^{-2} for the other cycles)

density. The rate capabilities of Si on 2D Cu and 3D Cu are shown in Fig. 4c. The discharge capacities of Si on 3D Cu shows superior capacities that are 2473, 1951, 1379 and 853 mAh g^{-1} at the current densities of 0.25, 0.50, 1.0 and 2.0 A g^{-1}, compared to Si on 2D Cu which shows capacities of 1714, 1302, 925 and 569 mAh g^{-1}, respectively. The discharge capacities of 2D Cu and 3D Cu are recovered to 698 and 1313 mAh g^{-1}, respectively, at the 40th cycle with current density of 1.0 A g^{-1}. The recovered capacity of 2D Cu (698 mAh g^{-1}) is far lower from the specific capacity at the earlier cycle (925 mAh g^{-1}) with same current density of 1.0 A g^{-1}. This phenomenon could be incurred by the detachment of silicon from the surface of 2D Cu. For better understanding of enhanced kinetics at 3D Cu, the charge/discharge profiles of the Si on 2D Cu and 3D Cu are shown in Fig. 5a-b. The cycle stability test of Si on 2D Cu and 3D Cu without the first 5 cycles are shown in Fig. 4d. Discharge capacities of Si on 2D Cu and 3D Cu are 1.86 mAh cm^{-2} and 2.07 mAh cm^{-2}, respectively, at the 6th cycle that is the first cycle with the current density of 1.0 A g^{-1}. Even though discharge capacity of the Si on 2D Cu at the 300th cycle is 0.16 mAh cm^{-2}, the Si on 3D Cu shows remarkable discharge capacity of 0.90 mAh cm^{-2}. This superior cycle stability of Si on 3D Cu is contributed by the increased area between active materials and CC that induces better electrical contacts between them.

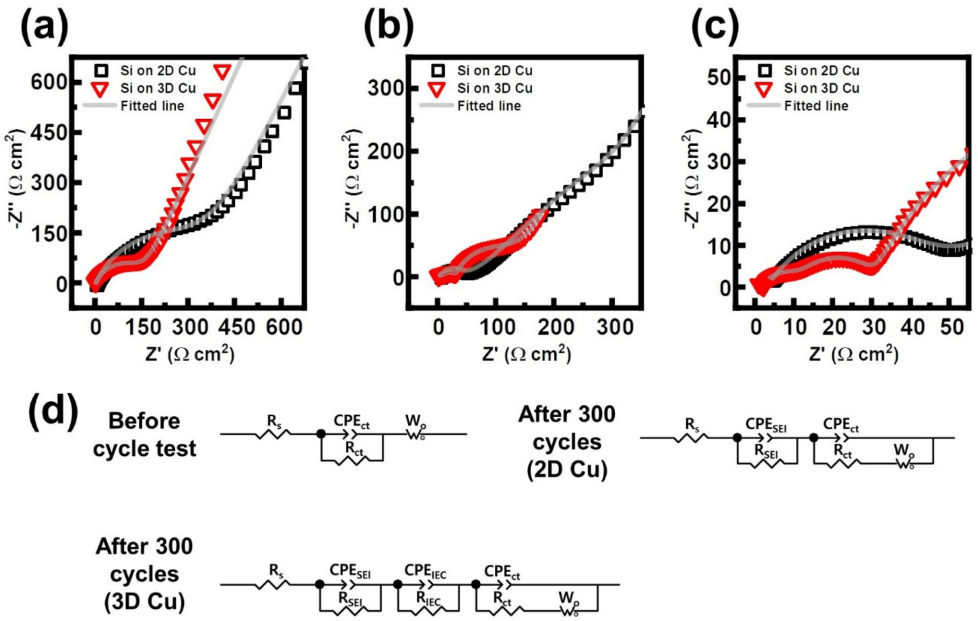

Fig. 6. EIS results of Si on 2D Cu and 3D Cu; Experimental and fitted curves before (a) cycle test, (b, c) after 300th cycle of Si on 2D Cu and 3D Cu with currents of 1 A g^{-1} corresponding to (d) the equivalent circuits

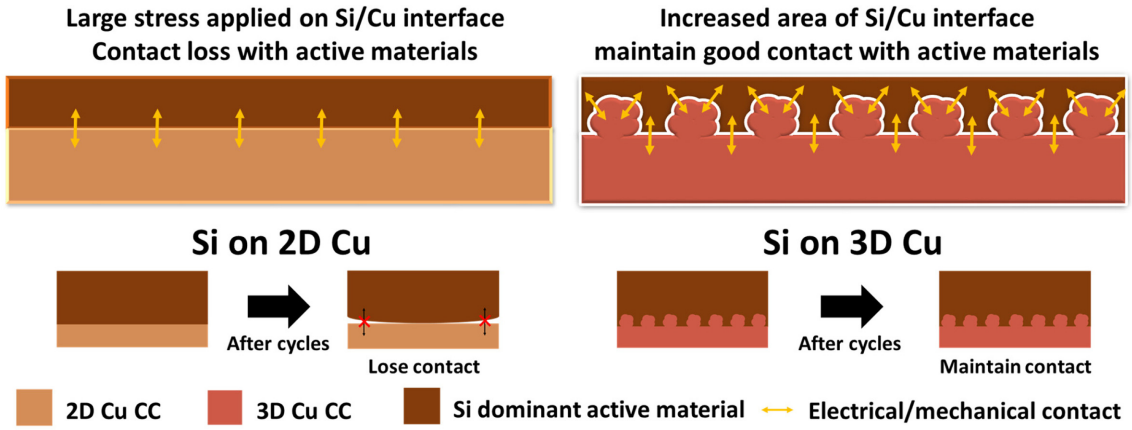

Fig. 7. The schematic representation showing the different contact area and adhesion strength with Si-dominant active materials between the conventional 2D Cu and the fabricated 3D Cu current collectors

To clarify the reason of superior cycle stability of Si on 3D Cu, the EIS results of Si on 2D Cu and 3D Cu before cycle stability test and after 300 cycles at 1 mA cm^{-2} are shown in Fig. 6a-c, and values of each of the resistances from the equivalent circuit (Fig. 6d) are shown in Table 1. R_s, R_{SEI}, R_{IEC} and R_{ct} are electrolyte resistance, SEI resistance, interphase electronic contact resistance, and charge transfer resistance, respectively. CPE_{SEI} and CPE_{ct} are constant phase elements (CPEs) corresponding to an imperfect double layer of an SEI and a film, respectively. The variable W_o is an open Warburg element in a low frequency alternating current condition. R_{IEC} and CPE_{IEC} are the interphase electronic contact resistance and CPE. The first semicircle associated with Si on 2D Cu is larger than Si on 3D Cu before cycle stability test. It means that the sum of R_s and R_{ct} at the 2D Cu is larger than R_e and R_{ct} at the 3D Cu. From Fig. 6b-c, there is a significant difference between the 2D Cu and 3D Cu after 300 cycles. The second semicircle at the high frequency occurs at the 3D Cu only and this semicircle is related to the new component, R_{IEC} and CPE_{IEC}. From the previous study, the R_{ct} at the high frequency is due to the weak contact between active material and conductive carbon, whereas R_{CAML} occurs at the high frequency when the contact between the CC and conductive carbon/binder system is tight [20].

Table 1. Values of internal resistances (R_s, R_{SEI}, R_{IEC} and R_{ct}) obtained through a fitting process based on Nyquist plots and equivalent circuits proposed in the EIS results (Fig. 3.)

	Before cycle		After 300 cycles	
	2D Cu	3D Cu	2D Cu	3D Cu
R_s / Ω cm^2	3.48	2.19	2.77	1.67
R_{SEI} / Ω cm^2	-	-	40.6	10.4
R_{IEC} / Ω cm^2	-	-	-	18.7
R_{ct} / Ω cm^2	330.3	151.1	126.1	119.6

Therefore, 3D Cu has large surface area that leads to the better electrical contact between the CC and carbon/binder system. Even though R_{IEC} is observed, the sum of all resistances at the 3D Cu are smaller than that at the 2D Cu. Moreover, all kinds of the resistances (R_s, R_{SEI} and R_{ct}) at the 3D Cu are lower than these values at the 2D Cu.

From the above results, we could conclude that 3D Cu improves the electrical conductivity of Si electrode and retains all kinds of binding among the anode components. These improvements lead to the higher cycle stability, the higher specific capacities and the lower overpotential of Si on 3D Cu compared with Si on 2D Cu. Enlarged surface area of 3D Cu could have enhanced all kinds of contacts and retaining the structure during the subsequent cycles, as shown in Fig. 7. We could conclude that enlarging surface area of Cu current collector is one of the effective strategies to improve electrochemical performances of Si electrodes, and it can be achieved by simple surface corrosion and subsequential thermal reduction.

4. Conclusions

The 3D Cu was successfully formed by a facile two-step synthesis using a combination method of chemical oxidation and thermal reduction. The fabricated 3D porous layer was composed of the porous Cu ball of which size was 3-5 μm, and its total thickness was 10.6 μm. It was notable that the 3D Cu was effective to alleviate the degradation of Si-dominant anode during LiB cycles due to the strengthened attachment of the active materials on a CC. Specifically, the Si electrode on 3D Cu could maintain a relatively high discharge capacity of 0.9 mAh cm^{-2} even after the 300th cycles (at 1.0 mA cm^{-2}), higher than that of 2D Cu (0.16 mAh cm^{-2}). It is because the electrical conductivity was improved attributed to a large contact area between active materials and CC, which could be confirmed from electrochemical analyses using CV and EIS.

Acknowledgments

This work was supported by GIST Research Institute (GRI) grant funded by Gwangju Institute of Science and Technology (GIST) in 2021.

References

1. U. Chang, J. T. Lee, J.-M. Yun, B. Lee, S. W. Lee, H.-I. Joh, K. Eom, and T. F. Fuller, In Situ Self-Formed Nanosheet Mos3/Reduced Graphene Oxide Material Showing Superior Performance as a Lithium-Ion Battery Cathode, *ACS nano*, **13**, 1490 (2018). Doi: https://doi.org/10.1021/acsnano.8b07191
2. G. Zubi, R. Dufo-López, M. Carvalho, and G. Pasaoglu, The Lithium-Ion Battery: State of the Art and Future Perspectives, *Renewable and Sustainable Energy Reviews*, **89**, 292 (2018). Doi: https://doi.org/10.1016/j.rser.2018.03.002
3. K. Eom, J. T. Lee, M. Oschatz, F. Wu, S. Kaskel, G. Yushin, and T. F. Fuller, A Stable Lithiated Silicon–Chalcogen Battery Via Synergetic Chemical Coupling between Silicon and Selenium, *Nature communications*, **8**, 13888 (2017). Doi: https://doi.org/10.1038/ncomms13888
4. D. Deng, M. G. Kim, J. Y. Lee, and J. Cho, Green Energy Storage Materials: Nanostructured Tio 2 and Sn-Based Anodes for Lithium-Ion Batteries, *Energy & Environmental Science*, **2**, 818 (2009). Doi: https://doi.org/10.1039/B823474D
5. J.-M. Tarascon and M. Armand, Issues and Challenges Facing Rechargeable Lithium Batteries, *Materials for sustainable energy: a collection of peer-reviewed research and review articles from Nature Publishing Group*, (2011). Doi: https://doi.org/10.1142/9789814317665_0024
6. S. Choi, T.-w. Kwon, A. Coskun, and J. W. Choi, Highly Elastic Binders Integrating Polyrotaxanes for Silicon Microparticle Anodes in Lithium Ion Batteries, *Science*, **357**, 279 (2017). Doi: https://doi.org/ 10.1126/science.aal4373
7. I. Kovalenko, B. Zdyrko, A. Magasinski, B. Hertzberg, Z. Milicev, R. Burtovyy, I. Luzinov, and G. Yushin, A Major Constituent of Brown Algae for Use in High-Capacity Li-Ion Batteries, *Science*, **334**, 75 (2011). Doi: https://doi.org/10.1126/science.1209150
8. J. Shin and E. Cho, Agglomeration Mechanism and a Protective Role of Al_2O_3 for Prolonged Cycle Life of Si Anode in Lithium-Ion Batteries, *Chemistry of Materials*, **30**, 3233 (2018). Doi: https://doi.org/10.1021/acs.chemmater.8b00145
9. Y. Han, P. Qi, J. Zhou, X. Feng, S. Li, X. Fu, J. Zhao, D.

Yu, and B. Wang, Metal–Organic Frameworks (Mofs) as Sandwich Coating Cushion for Silicon Anode in Lithium Ion Batteries, *ACS applied materials & interfaces*, **7,** 26608 (2015). Doi: https://doi.org/10.1021/acsami.5b08109

10. J. Liu, P. Kopold, P. A. van Aken, J. Maier, and Y. Yu, Energy Storage Materials from Nature through Nanotechnology: A Sustainable Route from Reed Plants to a Silicon Anode for Lithium-Ion Batteries, *Angewandte Chemie*, **127,** 9632 (2015). Doi: https://doi.org/10.1002/ange.201503150
11. H. Shang, Z. Zuo, L. Yu, F. Wang, F. He, and Y. Li, Low-Temperature Growth of All-Carbon Graphdiyne on a Silicon Anode for High-Performance Lithium-Ion Batteries, *Advanced Materials*, **30**, 1801459 (2018). Doi: https://doi.org/10.1002/adma.201801459
12. Y.-L. Kim, Y.-K. Sun, and S.-M. Lee, Enhanced Electrochemical Performance of Silicon-Based Anode Material by Using Current Collector with Modified Surface Morphology, *Electrochimica Acta*, **53**, 4500 (2008). Doi: https://doi.org/10.1016/j.electacta.2008.01.050
13. S.-H. Moon, S.-J. Kim, M.-C. Kim, J.-Y. So, J.-E. Lee, Y.-K. Shin, W.-G. Bae, and K.-W. Park, Stress-Relieved Si Anode on a Porous Cu Current Collector for High-Performance Lithium-Ion Batteries, *Materials Chemistry and Physics*, **223**, 152 (2019). Doi: https://doi.org/10.1016/j.matchemphys.2018.10.042
14. D. Ma, H. Zhou, J. Zhang, and Y. Qian, Controlled Synthesis and Possible Formation Mechanism of Leaf-Shaped Sns2 Nanocrystals, *Materials Chemistry and Physics*, **111**, 391 (2008). Doi: https://doi.org/10.1016/j.matchemphys.2008.04.035
15. X. Wen, W. Zhang, and S. Yang, Synthesis of Cu (Oh) 2 and Cuo Nanoribbon Arrays on a Copper Surface, *Langmuir*, **19**, 5898 (2003). Doi: https://doi.org/10.1021/la0342870
16. P. Xu, K. Ye, M. Du, J. Liu, K. Cheng, J. Yin, G. Wang, and D. Cao, One-Step Synthesis of Copper Compounds on Copper Foil and Their Supercapacitive Performance, *Rsc Advances*, **5**, 36656 (2015). Doi: https://doi.org/10.1039/C5RA04889C
17. C.-P. Yang, Y.-X. Yin, S.-F. Zhang, N.-W. Li, and Y.-G. Guo, Accommodating Lithium into 3d Current Collectors with a Submicron Skeleton Towards Long-Life Lithium Metal Anodes, *Nature communications*, **6**, 1 (2015). Doi: https://doi.org/10.1038/ncomms9058
18. J. A. Rodriguez, J. Y. Kim, J. C. Hanson, M. Pérez, and A. I. Frenkel, Reduction of Cuo in H 2: In Situ Time-Resolved Xrd Studies, *Catalysis Letters*, **85**, 247 (2003). Doi: https://doi.org/10.1023/A:1022110200942
19. K. Ogata, E. Salager, C. Kerr, A. Fraser, C. Ducati, A. J. Morris, S. Hofmann, and C. P. Grey, Revealing Lithium–Silicide Phase Transformations in Nano-Structured Silicon-Based Lithium Ion Batteries Via in Situ Nmr Spectroscopy, *Nature communications*, **5**, 3217 (2014). Doi: https://doi.org/10.1038/ncomms4217
20. J. Guo, A. Sun, X. Chen, C. Wang, and A. Manivannan, Cyclability Study of Silicon–Carbon Composite Anodes for Lithium-Ion Batteries Using Electrochemical Impedance Spectroscopy, *Electrochimica Acta*, **56**, 3981 (2011). Doi: https://doi.org/10.1016/j.electacta.2011.02.014